

# Simulating Galaxy Clusters - III: Properties of the Intracluster Stars

Jesper Sommer-Larsen<sup>1,2\*</sup>, Alessio D. Romeo<sup>1,2,3†</sup> and Laura Portinari<sup>1,4‡</sup>

<sup>1</sup>*Theoretical Astrophysics Center, Juliane Maries Vej 30, DK-2100 Copenhagen, Denmark*

<sup>2</sup>*Nordita, Blegdamsvej 17, DK-2100 Copenhagen, Denmark*

<sup>3</sup>*Dipartimento di Fisica e Astronomia, Università di Catania, via S.Sofia 64, 95123 Catania, Italy*

<sup>4</sup>*Tuorla Observatory, Väisäläntie 20, FIN-21500 Piikkiö, Finland*

Accepted —. Received —; in original form 2004 March 11

## ABSTRACT

TreeSPH simulations of the formation and evolution of galaxy groups and clusters have been performed in a standard  $\Lambda$ CDM cosmology. The simulations incorporate star-formation, chemical evolution with non-instantaneous recycling of gas and heavy elements, metal dependent radiative cooling, strong star-burst driven galactic superwinds, effects of a meta-galactic UV field and thermal conduction. Results for two clusters, one Virgo-like ( $T \simeq 3$  keV) and one (sub) Coma-like ( $T \simeq 6$  keV), are presented. At  $z=0$  the stellar contents of both clusters consist of a central dominant (cD) galaxy surrounded by cluster galaxies and intracluster stars. The intracluster (IC) stars are found to contribute 20-40% of the total cluster B-band luminosity at  $z=0$  and to form at a mean redshift  $\bar{z}_f \sim 3$  being on average about 0.5 Gyr older than the stars in cluster galaxies. UBVR<sub>I</sub>JHK surface brightness profiles of the IC star populations are presented; the profile of the larger cluster matches the observed V-band profile of the cD in Abell 1413 ( $T \simeq 8$  keV) quite well. The typical colour of the IC stellar population is B-R=1.4-1.5, comparable to the colour of larger elliptical galaxies. The mean Iron abundance of the IC stars is about solar in the central part of the cluster ( $r \sim 100$  kpc) decreasing to about half solar at the virial radius. The IC stars are  $\alpha$ -element enhanced with a weak trend of [O/Fe] increasing with  $r$  and an overall [O/Fe] $\sim 0.4$  dex.

The IC stars are kinematically significantly colder than the cluster galaxies: The velocity dispersions of the IC stars are in the inner parts of the clusters ( $r \sim 100$ -500 kpc) only about half of those of the cluster galaxies increasing slightly to about 70% at  $r=1$ -2 Mpc. The typical projected velocity dispersion in the Virgo-like cluster at  $R \gtrsim 50$  kpc is 300-600 km/s depending on orientation and projected distance from the cluster center. Rotation is found to be dynamically insignificant for the IC stars. The velocity distributions of IC stars *and* clusters galaxies are in one cluster highly radially anisotropic, in the other close to isotropic.

**Key words:** cosmology: theory — cosmology: numerical simulations — galaxies: clusters — galaxies: formation — galaxies: evolution

## 1 INTRODUCTION

Current hierarchical or “bottom-up” structure formation theories predict that the stellar haloes (the “field” stars) of galaxies like the Milky Way should consist partly of stars originally born in small proto-galaxies and later tidally stripped from these by the main galaxy or through inter-

action with other proto-galaxies. The fraction of the halo field stars of such origin depends (apart from obvious cosmic variance effects) on the properties of the dark matter (e.g., cold dark matter, CDM, vs. warm dark matter, WDM: for WDM the hierarchy is broken at the free-streaming mass scale) and the nature of the star-formation process. For example, some halo stars may be born in rapidly expanding, supernova driven proto-galactic supershells and hence be detached from their parent proto-galaxies right from the outset in space, as well as phase-space (e.g., Mori et al. 1997; Sommer-Larsen, Götz & Portinari 2003). If dark matter

\* E-mail: jslarsen@tac.dk

† E-mail: aro@ct.astro.it

‡ E-mail: lportina@tac.dk

is cold and star-formation in expanding supershells is not a common phenomenon the above fraction could be quite large, in principle at least, approaching unity (e.g., Helmi et al. 2003). The halo stars resulting from tidal stripping or disruption of a proto-galaxy will stay localized in phase-space for a long period and several such “streams” of halo stars have been detected in the haloes of the Milky Way and M31 (e.g., Helmi et al. 1999; Ferguson et al. 2002).

From the point of view of structure formation, galaxy clusters can be seen as scaled up versions of galaxies in hierarchical scenarios. In particular, gravity is expected to strip or disrupt cluster galaxies in a similar way as in galaxy haloes and a population of intracluster (or “field”) stars should thus reside between the cluster galaxies. It has been known for decades that cD galaxies often are embedded in extended envelopes presumed to be stars tidally stripped off galaxies in the process of being engulfed by the cD (e.g., Oemler 1976; Dressler 1979). In recent years it has been possible to perform quantitative studies of these stellar envelopes through ultra-deep surface photometry of the general stellar population (e.g., Gonzalez et al. 2000; Feldmeier et al. 2002), or imaging/spectroscopy of individual planetary nebulae (e.g., Arnaboldi et al. 2002, 2003) or supernovae Type Ia (Gal-Yam et al. 2003).

On the theoretical front Napolitano et al. (2003) have used an N-body dark matter only fully cosmological simulation of the formation of a Virgo-like cluster to make predictions about intracluster stars. They find that unrelaxed velocity distributions and (bulk) streaming motions of the IC stars should be common due to the large dynamical timescales in clusters. Hence the evolution towards a relaxed coarse-grained phase-space distribution function through phase-mixing has proceeded much less far<sup>1</sup> than, e.g., in the Galactic halo, where dynamical timescales are much shorter.

The dark matter only simulations are complemented by various N-body simulations which invoke a more realistic modelling of the stellar properties of galaxies in order to study the fate of galaxies in a cluster environment (e.g., “galaxy harassment”, Moore et al. 1996, “tidal stirring”, Mayer et al. 2001 and the formation of the central cluster galaxy, Dubinski 1998). The advantage of this approach is that a very high resolution in the stellar component can be obtained.

In general the properties of the system of IC stars are set by two main effects: a) the cool-out of gas and subsequent conversion of cold, high-density gas to stars in individual galaxies and b) the stripping/disruption of the galaxies through interactions with other galaxies and the main cluster potential. Since the latter interactions will generally affect the star-formation rate (as long as a reservoir of gas is available) the former process is intimately coupled to the latter.

Only fairly recently has it been possible to carry out fully cosmological gas-dynamical/N-body simulations of the formation and evolution of galaxy clusters at a level of numerical resolution and physical sophistication that the cool-out of gas, star-formation and chemical evolution in and

outflows from individual cluster galaxies can be modelled to, at least some, degree of realism (e.g., Valdarnini 2003; Tornatore et al. 2004). Recently Murante et al. (2004) analyzed 117 clusters formed in a large cosmological TreeSPH simulation (Borgani et al. 2004) to study the properties of the IC stars. They determined average density profiles of the IC stars as well as stars in galaxies for their large sample of clusters. One of the interesting conclusions reached is that only at fairly large cluster-centric distances ( $r \gtrsim 0.4-0.5r_{\text{vir}}$ ) does the density of stars in galaxies (excluding the cD) exceed that of IC stars.

We have recently engaged in undertaking similar simulations of galaxy groups and clusters. We are building on our TreeSPH code used for simulating galaxy formation (e.g., Sommer-Larsen, Götz & Portinari 2003), improved to include modelling of non-instantaneous chemical evolution (Lia, Portinari & Carraro 2002), metal-dependent, atomic radiative cooling, strong (supernova or AGN driven) galactic winds and thermal conduction. The main results will be described elsewhere (Romeo et al. 2004) — in this paper we present our first results on the properties of the IC stars in two simulated clusters, one Virgo-like and one Coma-like. Our results complement those of Murante et al. (2004), since we present for the IC stars also results on multiband surface brightness profiles, colours, abundances and detailed kinematics.

In section 2 we briefly describe the code and the numerical simulations, in section 3 we present and discuss the results obtained, and finally section 4 constitutes our conclusions.

## 2 THE CODE AND SIMULATIONS

The code used for the simulations is a significantly improved version of the TreeSPH code used previously for galaxy formation simulations (Sommer-Larsen, Götz & Portinari 2003): Firstly, in lower resolution regions (which will always be present in cosmological CDM simulations) an improvement in the numerical accuracy of the integration of the basic equations can be obtained by solving the entropy equation rather than the thermal energy equation — we have adopted the “conservative” entropy eq. solving scheme suggested by Springel & Hernquist (2003). Secondly, non-instantaneous chemical evolution tracing 9 elements (He, C, N, O, Mg, Si, S, Ca and Fe) has been incorporated in the code following Lia, Portinari & Carraro (2002). Atomic radiative cooling depending both on the metal abundance of the gas and the meta-galactic UV field is invoked together with simplified radiative transfer. Thirdly, star-burst driven, galactic super-winds are incorporated in the simulations. This is required to get the abundance of the ICM to the observed level of about 1/3 solar in iron. The strength of the super-winds is modelled through a free parameter  $f_{\text{wind}}$  which determines how large a fraction of the stars born partake in super-wind driving star formation. We find that in order to get an iron abundance in the ICM comparable to observations,  $f_{\text{wind}} \gtrsim 0.5$  and at the same time a fairly top-heavy Initial Mass Function (IMF) has to be used. Finally, thermal conduction was implemented in the code following Cleary & Monaghan (1999).

We ran simulations of two small and two larger galaxy

<sup>1</sup> A visualized example from one of our simulations is given at <http://www.tac.dk/~jls Larsen/ICstars>

groups as well as a Virgo-like and a (mini) Coma-like cluster — we shall denote the latter two clusters C1 and C2 in the following. All 6 systems were chosen to be fairly relaxed (no  $\gtrsim 1:2$  merging at  $z \lesssim 1$ ). Virial masses at  $z=0$  were approximately  $3.4 \times 10^{13}$ ,  $7.9 \times 10^{13}$ ,  $2.0 \times 10^{14}$  and  $8.4 \times 10^{14} h^{-1} M_{\odot}$  and (X-ray) emission weighted temperatures 1.1, 1.6, 3.0 and 6.0 keV, respectively. The groups and clusters were selected from a cosmological, DM-only simulation of a flat  $\Lambda$ CDM model, with  $\Omega_M=0.3$ ,  $\Omega_b=0.036$ ,  $h=0.7$  and  $\sigma_8=0.9$  and a box-length of  $150 h^{-1}$  Mpc. Mass and force resolution was increased in Lagrangian regions enclosing the groups and clusters, such that  $m_{\text{gas}}=m_*=2.5 \times 10^8$  and  $m_{\text{DM}}=1.8 \times 10^9 h^{-1} M_{\odot}$  for the high resolution gas, star and dark matter particles. Particle numbers are in the range 100000-500000 SPH+DM particles. Gravitational (spline) softening lengths of  $\epsilon_{\text{gas}}=\epsilon_*=2.8$  and  $\epsilon_{\text{DM}}=5.4 h^{-1}$  kpc, respectively, were adopted. The gravity softening lengths were fixed in physical coordinates from  $z=6$  to  $z=0$  and in comoving coordinates at earlier times. To test for numerical resolution effects one simulation was run with eight times higher mass and two times higher force resolution, yielding  $m_{\text{gas}}=m_*=3.1 \times 10^7$  and  $m_{\text{DM}}=2.3 \times 10^8 h^{-1} M_{\odot}$  and gravity softening lengths of 1.4, 1.4 and  $2.7 h^{-1}$  kpc, respectively.

Cold high-density gas is turned into stars in a probabilistic way as described in Sommer-Larsen, Götz & Portinari (2003). In a star-formation event an SPH particle is converted fully into a star particle. Non-instantaneous recycling of gas and heavy elements is described through probabilistic “decay” of star particles to SPH particles as discussed by Lia, Portinari & Carraro (2002). In a decay event a star particle is converted fully into an SPH particle.

For the simulation presented in this paper  $f_{\text{wind}}=0.7$ , and an Arimoto-Yoshii IMF (e.g., Lia, Portinari & Carraro 2002) was adopted, and AGN driven winds were not invoked. Moreover, the thermal conductivity was set to zero assuming that thermal conduction in the ICM is highly suppressed by magnetic fields (e.g., Etori & Fabian 2000).

### 3 RESULTS AND DISCUSSION

In this section we present and discuss results for clusters C1 and C2 run at our “standard” resolution. As mentioned above, we also performed a test simulation at 8 times higher mass and 2 times better force resolution; for computational reasons this was run for one of our galaxy groups. Some of the results of this test will be presented at the end of this section, but the general indication of the test is that none of the following results concerning mass and luminosity fractions, mean ages, surface brightness profiles, colours, abundances, kinematics and density profiles of the IC stars change in any significant way with increased numerical resolution.

All results presented in the following refer to  $z=0$ , unless another epoch is explicitly specified. At  $z=0$   $1.2 \times 10^4$  and  $2.3 \times 10^4$  star particles are located inside of  $r_{\text{vir}}=1.3$  and  $2.0 h^{-1}$  Mpc of the clusters C1 and C2. The corresponding mass in stars is  $2.9 \times 10^{12}$  and  $5.6 \times 10^{12} h^{-1} M_{\odot}$  or a fraction of about 1% of the total virial mass (the stellar mass fraction is smaller for C2 than for C1 - we shall return to this below). In both clusters the stellar mass constitutes 14% of the total baryonic mass inside of the virial radius. In the following we shall refer to star particles simply as “stars”.

The stellar contents of both clusters are characterized by a massive, central dominant (cD) galaxy surrounded by galaxies and intracluster stars. The effective radii of the two cD galaxies are  $R_{\text{eff}} \simeq 5$  kpc (taking the inner 80 kpc of the cluster as the extent of the cD — see below) in reasonable agreement with observational estimates (e.g., Feldmeier et al. 2002). For a study of the formation of the brightest cluster galaxy (BCG) based on a pure N-body simulation (but of higher resolution than ours) Dubinski (1998) found an effective radius of  $\sim 20$  kpc for the central BCG - we shall return to this below.

#### 3.1 Identifying Cluster Galaxies and Intracluster Stars

The first step in identifying the IC stars is to find all galaxies in the clusters. To this end we proceed in the following simple way: by visual inspection of the  $z=0$  frames the stars in all galaxies except the cD are located within 10-15 kpc from the centers of the galaxies. A cubic grid of cube-length  $\Delta l=10$  kpc is overlaid the cluster, and all cubes containing at least  $N_{\text{th}}=2$  stars are identified. Subsequently, each selected cube is embedded in a larger cube of cube-length  $3\Delta l$ . If this larger cube contains at least  $N_{\text{min}}=7$  star particles, which are gravitationally bound by its content of gas, stars and dark matter the system is identified as a potential galaxy. Since the method can return several, almost identical versions of the same galaxy only the potential galaxy of these containing the largest number of star particles is kept and classified as a galaxy. We tested the galaxy identification algorithm by varying  $\Delta l$ ,  $N_{\text{th}}$ ,  $N_{\text{min}}$ , and also the numerical resolution of the simulations (see below) and found it to be adequately robust for the purposes of this paper.

The algorithm identifies  $N_{\text{gal}}=42$  and 94 galaxies inside of the virial radii of C1 and C2, respectively, plus a cD at the center of each cluster. The reason why the ratio  $N_{\text{gal}}(\text{C2})/N_{\text{gal}}(\text{C1})$  is somewhat less than the ratio of the corresponding virial masses is discussed below. Apart from the cD there are no galaxies inside of  $r_{\text{cD}}=80$  kpc in either of the  $z=0$  frames (this is not true in all  $z \sim 0$  frames for clusters C1 and C2, though, but we tested that the results we present in the following did not depend on which  $z \sim 0$  frame was chosen to represent the present epoch — see also below).

We define the system of IC stars as the stars located at cluster-centric distances  $r_{\text{cD}} \leq r \leq r_{\text{vir}}$  and *not* inside of the tidal radius (e.g., Binney & Tremaine 1987) of any galaxy in the cluster. The cD itself is effectively just the inward continuation of the system of IC stars and the division between IC stars and cD is somewhat arbitrary (we hence below quote intracluster star fractions for  $r_{\text{cD}}=80$  as well as 40 kpc). The above definition is conservative, since we calculate the tidal radii on the basis of the  $z=0$  frame cluster-centric distances of the galaxies. This tidal radius should for any galaxy which has been through at least one peri-center passage be taken as a firm upper limit. Moreover, some IC stars will be inside of the tidal radius of one of the cluster galaxies just by chance. As the total “tidal volume” of all the cluster galaxies is found to be a few tenth of a percent of the virial volume of the cluster this effect can be neglected, however.

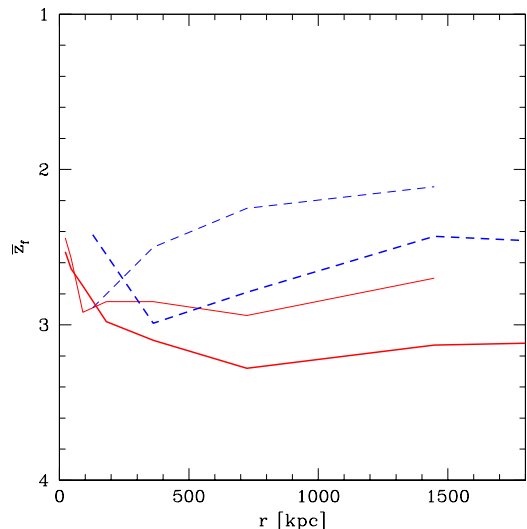


**Figure 1.** Mean redshift of formation of the cD + IC stars (solid lines) and stars in galaxies (dashed lines) at  $z=0$ . Results for cluster C1 (“Virgo-like”) are shown by thin lines and for C2 (“mini-Coma”) by heavy lines. Statistical uncertainties are  $\Delta\bar{z}_f \lesssim 0.05$ .

### 3.2 The Intracluster Star Fraction

Using the above definition we find that the intracluster stars constitute 21 and 28% of the stellar mass inside of the virial radius for clusters C1 and C2, respectively (adopting  $r_{\text{cD}}=40$  kpc these numbers increase slightly to 28 and 34%). For comparison with observations it is more relevant to look at stellar luminosities. Since ages and metallicities are available for all star particles, the photometric properties are straightforward to calculate treating each star particle as a Single Stellar Population (SSP). SSP luminosities are computed by mass-weighted integration of the Padova isochrones (Girardi et al. 2002), according to the Arimoto-Yoshii IMF. We find that the IC stars contribute only 9 and 11% of the cluster B-band luminosities for C1 and C2 respectively. This is significantly less than the observational estimate of  $L_{\text{B,IC}}/L_{\text{B,tot}} \gtrsim 0.2$  (e.g., Arnaboldi 2004). The likely reason for this discrepancy is an excess of stars formed fairly recently at the center of the cD and dominating the B-band luminosity: After a period of major merging at  $z \sim 1-2$  strong, quasi-stationary cooling flows develop at the centers of the clusters despite the strong, super-nova driven energy feedback to the IGM/ICM through galactic super-winds and the use of a fairly top-heavy IMF. As a consequence, stars continue to form steadily at the centers of the cDs ( $r \lesssim 10$  kpc). At  $z=0$  the cDs are too blue compared to observed cDs with central B-R colours of  $\sim 1.0$  (see Fig. 4) rather than 1.4-1.5 (note though that some star-formation is observed in many cDs at the base of the cooling flow — e.g., McNamara 2004). To make a (albeit crude) correction for this excess of young stars at the centers of the simulated cDs we temporarily discard the luminosity contribution of all stars in the inner  $r_c=10$  kpc with formation redshifts  $z_f < z_c$ , where  $z_c$  is determined by requiring that the mean forma-

tion redshift of the remaining stars inside of  $r_c$  should be similar to the mean formation redshift of stars at  $r \gtrsim r_c$ . We find that this is the case for  $z_c \sim 1$  and shall in the following in various cases present results with and without this crude correction, adopting  $z_c=1$  for the former. With this correction  $L_{\text{B,IC}}/L_{\text{B,tot}}=0.29$  and  $0.42$  for the two clusters in better agreement with observations (for  $r_{\text{cD}}=40$  kpc we obtain  $L_{\text{B,IC}}/L_{\text{B,tot}}=0.42$  and  $0.50$ , respectively). Moreover, the effective radii of the cDs increase to 9 and 11 kpc, respectively. These values are also in reasonable agreement with observations (Feldmeier et al. 2002) and in better agreement with the finding of Dubinski (1998), but still somewhat smaller. This seems reasonable, since Dubinski’s simulation was pure N-body (i.e. completely non-dissipative).

### 3.3 Mean Formation Redshifts, Surface Brightness Profiles and Colours of the Intracluster Stars

In Figure 1 we show the mean (spherically averaged) redshift of formation,  $\bar{z}_f$ , of the cD + IC stars (solid lines) and stars in galaxies except the cD (dashed lines) as a function of radial distance from the center of the cD for clusters C1 and C2, respectively. For both clusters the average formation redshift of the IC stars is  $\bar{z}_{f,IC} \sim 3$  at  $r \gtrsim 100-200$  kpc. The stars in galaxies (except the cD) are on average somewhat younger with  $\bar{z}_{f,gal} \sim 2.5$ . This is to be expected, since the bulk of the IC stars originate in (proto) galaxies, which have been partly or fully disrupted through tidal stripping in the main cluster potential or by galaxy-galaxy interactions. In contrast, the galaxies still remaining at  $z=0$  have potentially been able to continue forming stars from cold gas remaining since the formation of the galaxy or gas recycled by evolved stars and subsequently cooled to star-forming temperatures and densities. Due to ram-pressure stripping and other effects the star-formation rate in the galaxies decreases significantly from  $z=2$  to 0, however, considerably more so than in field galaxies (Romeo et al. 2004). Murante et al. (2004) find a similar trend that the IC stars are on average older than the stars still in cluster galaxies, but they find significantly lower mean redshifts of formation,  $\bar{z}_f=1.5$  and  $1.2$  respectively. The reason for this discrepancy is not clear: it may be related to different galactic super-wind prescriptions or that we incorporate metal-dependent radiative cooling in the simulations, whereas Borgani et al. (2004) use a primordial cooling function, but is probably not due to numerical resolution differences (Murante 2004, private communication).

From Figure 1 it can be seen that the IC stars as well as stars in galaxies in cluster C2 are on average somewhat older than those in C1. The reason for this is numerical, rather than physical: When preparing the initial conditions for C2 we had for computational limitations to use a volume somewhat smaller than the “virial volume” for the (high resolution) region which is represented by both SPH and dark matter particles. The volume outside of this region is represented by dark matter particles only. These dark matter particles have close to SPH/DM region a mass comparable to the dark matter particles in the SPH/DM region (a factor  $1/(1-f_b)$  larger, where  $f_b$  is the universal baryon fraction) and the dark matter only volume is increasingly coarsely sampled with increasing distance from the SPH/DM region.

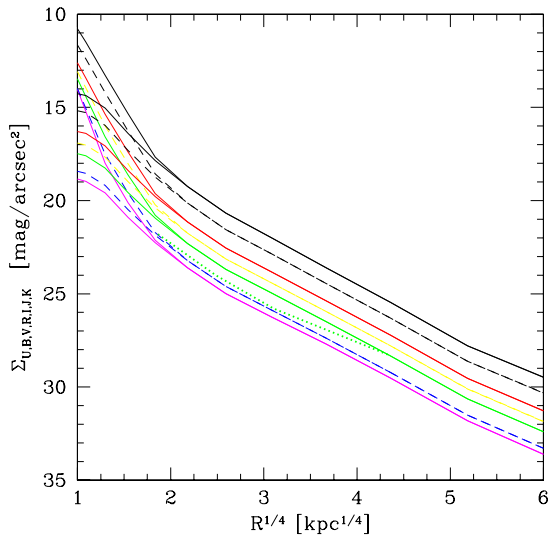


**Figure 2.** Multiband (UBVRIJK going bottom up) surface brightness profiles of cD + IC stars for cluster C2, shown with (thin lines) and without (thicker lines) the correction for the excess young, central stars, discussed in the text. Also shown (thick dotted line) is V-band surface photometry for the cD in the rich cluster A1413 ( $T \simeq 8$  keV) obtained by Feldmeier et al. 2002

As a consequence of these sampling limitations about half of the mass inside of the virial radius of the final cluster is in the form of dark matter particles which are still of high resolution, but have not been split into SPH and DM particles. The relative importance of these “non-split” dark matter particles increases with radius in the cluster. In general, the amount of late infall of gas and galaxies is reduced compared to the fully resolved case — this explains the somewhat larger age of the C2 stars relative to the C1 stars. It also explains why the mass of stars in C2 is about two times and not four times that of the stars in C1 and why  $N_{\text{gal}}(\text{C2})/N_{\text{gal}}(\text{C1})$  is only about two, as mentioned at the beginning of this section.

In Figure 2 we show for cluster C2 the azimuthally averaged UBVRIJK surface brightness profiles of the cD+IC stars, both with and without the correction discussed above. The orientation is such that the cD is viewed along the minor axis, but other orientations give very similar results. The light profiles are approximately described by  $r^{1/4}$  laws. In reality the slope flattens with increasing  $r$ , so the system can be seen as a central dominant elliptical galaxy surrounded by an extended envelope, with the slope of the surface brightness profile becoming close to constant beyond  $r \sim 40$  kpc. These are characteristics of observed cD galaxies (e.g., Feldmeier et al. 2002). Observationally, cD+IC stars can be traced by surface photometry to  $V_{\text{lim}} \simeq 28.3$  mag/arcsec<sup>2</sup> (e.g., Feldmeier et al. 2002), which for cluster C2 corresponds to  $r \sim 350$  kpc. In Figure 2 we also show V band surface photometry of the cD + envelope in the rich cluster A1413 ( $T \simeq 8$  keV) obtained by Feldmeier et al. (2002). Though the observational V band profile is slightly flatter than what we predict for the V band, overall agreement is

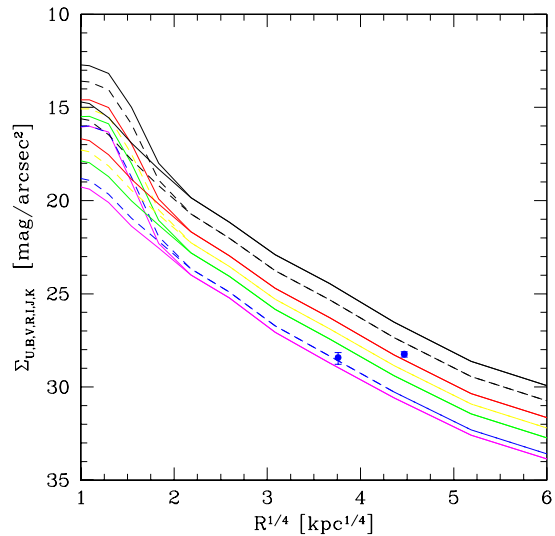


**Figure 3.** Same as in Figure 2, but now for cluster C1. Data points are B-band IC star estimates based on planetary nebulae observations in the Virgo cluster by Arnaboldi et al. 2002

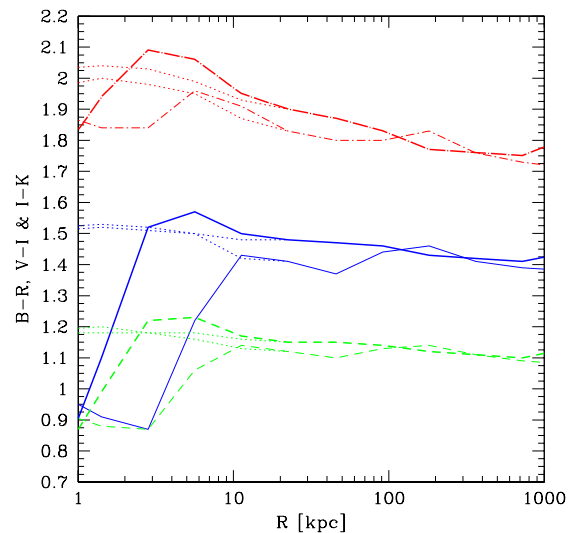


**Figure 4.** Azimuthally averaged B-R (solid lines), R-I (dashed lines) and I-K (dot-dashed lines) colours of cD + IC stars for clusters C2 (thick lines) and C1 (thinner lines), respectively. The results of applying the correction for the excess, central young stars is shown with thin dotted lines.

quite good, especially when it is taken into account that the sampling of the baryons becomes increasingly incomplete with radius in cluster C2 (see above). In Figure 3 we show the surface brightness profiles of C1 (“Virgo”). Also shown is two B-band data points derived for Virgo IC stars (indirectly) using planetary nebulae by Arnaboldi et al. (2002).

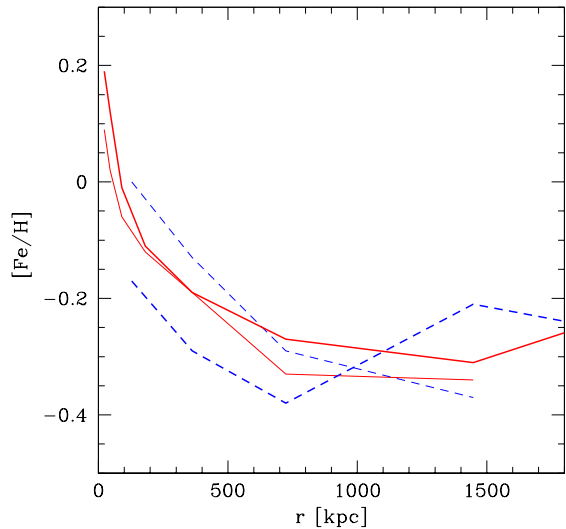


**Figure 5.** Spherically averaged iron abundance of cD+IC stars (solid lines) and stars in cluster galaxies (dashed lines) for clusters C1 (thin lines) and C2 (thick lines), respectively.

Our predicted B-band profile fits the inner point well, but not the outer one, which is too high (in fact slightly higher than the inner one). The Virgo cluster is known, however, to have an unusually flat galaxy surface brightness profile and possibly be dynamically unrelaxed (Binggeli et al. 1987), so this may not be entirely surprising.

Shown in Figure 4 are the azimuthally averaged B-R, R-I and I-K colours of the cD+IC stars, again with and without the correction discussed above. Outside about 10 kpc the colours are typical of the stellar population in larger elliptical galaxies with  $B-R=1.4-1.5$  (e.g., Gladders et al. 1998), in qualitative agreement with the observational findings of Gonzalez et al. (2000) for the rich cluster Abell 1651. Within 10 kpc this is also the case when the correction for the excess of central, young stars has been applied — if not, the core of the cD gets too blue with central colours approaching those of spiral galaxies. Outside of 10 kpc the colour of the cD+IC stars gets bluer with increasing  $R$ . As the mean age of the stars is approximately constant with  $R$  (see Fig. 1), this is mainly due to a decrease in metal abundance with  $R$  (see below).

### 3.4 Abundance Properties of the Intracluster Stars and Cluster Galaxies

In Figure 5 we show the spherically averaged iron abundance of the cD+IC stars as well as stars in cluster galaxies as a function of cluster-centric distance. Iron is super-solar in the cD+IC stars at  $r \lesssim 100$  kpc and decreases to about half solar at large  $r$ . It follows from Fig. 5 that the stars in cluster galaxies follow a similar trend. The fairly large overall iron abundance of the IC stars, as compared to, e.g., stars in the halo of the Milky Way, reflects that it is the galaxies (past and present) which have to enrich the 5-10 times more massive hot intracluster medium (ICM) to an iron abun-

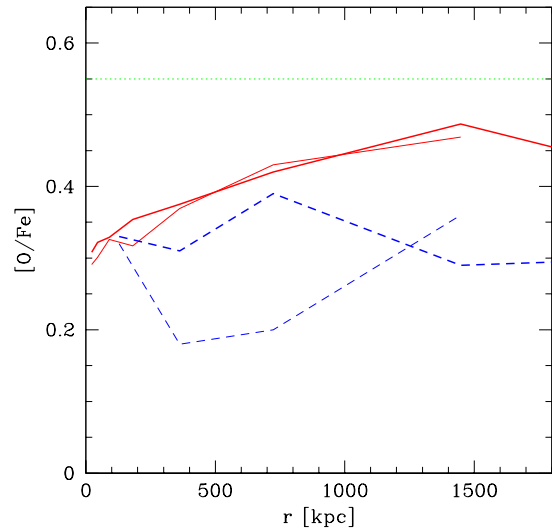


**Figure 6.** Spherically averaged oxygen-to-iron abundance ratio of cD+IC stars (solid lines) and stars in cluster galaxies (dashed lines) for clusters C1 (thin lines) and C2 (thick lines), respectively. The limiting case for pure SNII enrichment  $[O/Fe]=0.55$  is shown by the thin, dotted line.

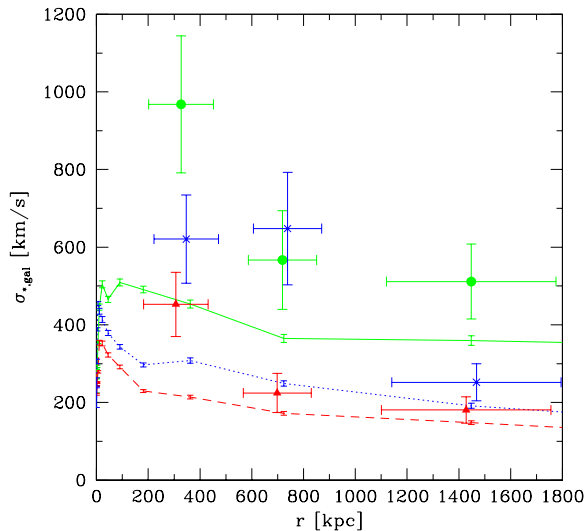
dance of about 1/3 solar (Romeo et al. 2004). Durrell et al. (2002) carried out HST observations of an IC field in the Virgo cluster at an average projected distance of 150 kpc from M87 (which for the purposes here can be assumed coincident with cluster center). They confirm an excess of red number counts, which they interpret as IC RGB stars. By comparison with observations of a dwarf irregular, they conclude that these stars have  $-0.8 < [Fe/H] < -0.2$ . Though this is somewhat less than we predict, the discrepancy is only a factor of about two, and the observational abundances are clearly significantly larger than those of the halo stars of the Milky Way.

Figure 6 shows the corresponding oxygen-to-iron ratios as a function of  $r$ .  $[O/Fe]$  is super-solar everywhere. This is in agreement with present estimates for the luminous elliptical galaxies that contain most of the stellar mass in cluster galaxies. For the IC stars no observational information is currently available (Arnaboldi 2004, private communication).

For enrichment by supernovae type II only one expects for the Arimoto-Yoshii IMF  $[O/Fe]_{\text{SNII}}=0.55$  (e.g., Lia, Portinari & Carraro 2002), so it follows from Fig. 6 that SNe Ia do contribute somewhat to the enrichment of the cD+IC stellar populations, and (not surprisingly) even more so for the stars still in galaxies at  $z=0$  (in fact for an Arimoto-Yoshii IMF the global ( $t \rightarrow \infty$ ) value of the SNII+SN Ia enrichment is  $[O/Fe]=0.18$ ).

### 3.5 Kinematics of the Intracluster Stars and Cluster Galaxies

Using observed velocities of planetary nebulae it will ultimately be possible to kinematically “dissect” the systems of



**Figure 7.** For cD+IC stars in cluster C1 is shown velocity dispersions  $\sigma_r$  (solid lines),  $\sigma_\phi$  (dotted line) and  $\sigma_\theta$  (dashed line). The statistical uncertainties are marked with small errorbars. The similar quantities are shown for the cluster galaxies by filled circles, crosses and filled triangles, with larger errorbars marking the statistical uncertainties.

cD+IC stars in nearby galaxy clusters, such as Virgo. It is hence of considerable interest to determine for our simulations the velocity distribution of the cD+IC stars and compare it to that of cluster galaxies. To this end we proceed as follows: At  $z=0$  cluster C1 and the cD at the center are somewhat flattened (ellipticity  $\epsilon = 1 - b/a \simeq 0.4$ ) with similar minor axis orientations (we shall denote the minor axis of the cD the “z-axis” in the following). Cluster C2 is only slightly flattened ( $\epsilon \simeq 0.2$ ), and so is the cD at the center, with approximately perpendicular minor axis orientations. For each cD+IC star and each cluster galaxy we determine three perpendicular velocity components: The radial component  $v_r = \vec{v} \cdot \vec{e}_r$ , where  $\vec{e}_r$  is the unit vector pointing radially away from the center of the cluster, the perpendicular (tangential) component  $v_\phi = \vec{v} \cdot \vec{e}_\phi$ , where  $\vec{e}_\phi$  is the unit vector perpendicular to  $\vec{e}_r$  and aligned with the x-y plane and the third (tangential) component  $v_\theta = \vec{v} \cdot \vec{e}_\theta$ , where  $\vec{e}_\theta$  is the unit vector  $\vec{e}_\theta = \vec{e}_r \times \vec{e}_\phi$ .

We calculate the mean rotation  $\bar{v}_\phi$  and velocity dispersions  $\sigma_r$ ,  $\sigma_\phi$  and  $\sigma_\theta$  of cD+IC stars and galaxies in spherical shells. Outside  $r \sim 10$  kpc rotation is found to be dynamically insignificant with  $\bar{v}_\phi \lesssim 20$ -40 km/s in both clusters. When correcting for the excess young, central stars rotation is found to be also dynamically unimportant at  $r < 10$  kpc. In Figures 7 and 8 we show the velocity dispersions of the cD+IC stars and cluster galaxies in clusters C1 and C2, respectively, versus cluster-centric distance. The cD+IC stars are kinematically significantly colder than the cluster galaxies: The velocity dispersions of the cD+IC stars are in the inner parts of the clusters ( $r \sim 100$ -500 kpc) only about half of those of the cluster galaxies, increasing slightly to about 70% at  $r \sim 1$ -2 Mpc. As stars and galaxies are moving in the

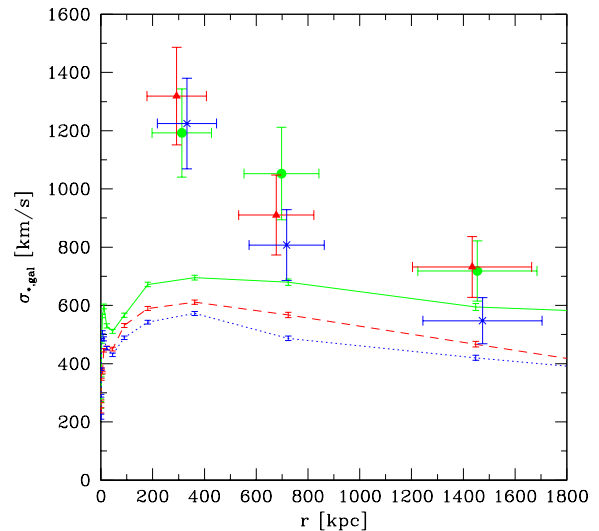


**Figure 8.** Same as Figure 7, but for cluster C2.

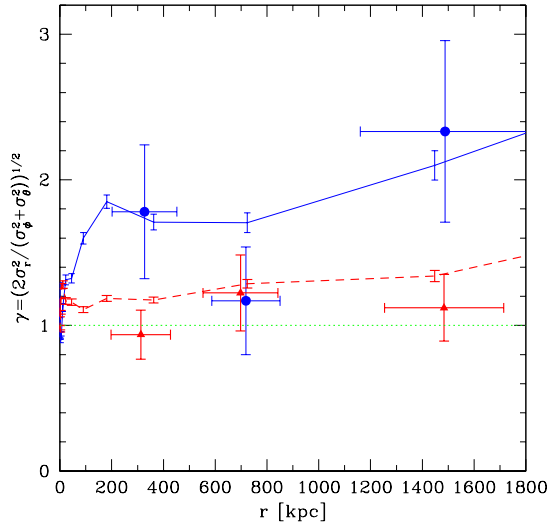


**Figure 9.** Velocity anisotropy parameter  $\gamma$  for cD+IC stars (solid line) and galaxies (solid circles) for cluster C1. The same is shown for cluster C2 by dashed line and solid triangles. An isotropic velocity distribution has  $\gamma=1$  indicated by a thin, dotted line.

same gravitational potential this implies by Jean’s theorem (e.g., Binney & Tremaine 1987) that the (number) density distribution of cluster galaxies is significantly flatter than that of cD+IC stars, in particular in the inner parts of the clusters — see below.

The velocity distribution of the cD+IC stars in cluster C1 is highly radially anisotropic at  $r \gtrsim 100$  kpc, and, within the statistical uncertainties, this is also the case for the cluster galaxies. We quantify this in Figure 9, where we show



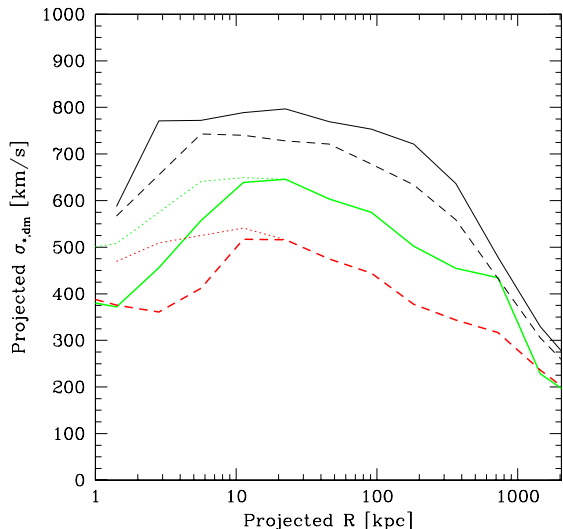


**Figure 10.** Projected velocity dispersions for cluster C1 of cD+IC stars (thick lines) and dark matter (thinner lines) along the minor axis (z-axis; dashed lines) and averaged along the x and y-axis (solid lines) of the cD/cluster. Thin dotted lines mark the effect of making the correction for the excess young central stars. Statistical uncertainties are  $\Delta\sigma \lesssim 20$  km/s.

the ratio  $\gamma = \sqrt{(2\sigma_r^2/(\sigma_\phi^2 + \sigma_\theta^2))}$ , where  $\gamma^2$  is the ratio of the kinetic energy in radial and mean tangential (1D) motions, respectively. For an isotropic velocity distribution  $\gamma=1$ . In cluster C1 there is almost twice as much kinetic energy in the radial direction than in the sum of the two tangential directions at  $r \gtrsim 100$  kpc. Interestingly, within the statistical uncertainties the same appears to hold for the galaxies, which at first seems surprising, since one would expect that it is predominantly galaxies on radial orbits which are tidally disrupted and transformed into cD+IC stars. The explanation for this lack of difference in the orbital characteristics of the two populations is likely the combined effect of radial infall of and dynamical friction on cluster galaxies, but we defer a detailed discussion of this to a forthcoming paper. In cluster C2 the velocity distribution of the cD+IC stars is only mildly radially anisotropic and the velocity distribution of the cluster galaxies is, within the statistical uncertainties, isotropic.

Finally, concerning the flattening of the systems for cluster C1  $\sigma_\phi$  is about 50% larger than  $\sigma_\theta$  for cD+IC stars as well as galaxies, indicating that these systems are flattened by anisotropic velocity distributions — see below. For cluster C2  $\sigma_\phi \simeq \sigma_\theta$ , consistent with this cluster being only mildly flattened.

Observationally one will for the cD+IC stars only be able to determine line-of-sight velocities using planetary nebulae, not full 3D velocities. For direct comparison with observations we show in Figure 10 the projected velocity dispersions of the cD+IC stars and (for comparison) of the dark matter in cluster C1 versus projected distance from the center of the cD. By dashed lines we show the azimuthally averaged velocity dispersions along the minor axis of the cD.

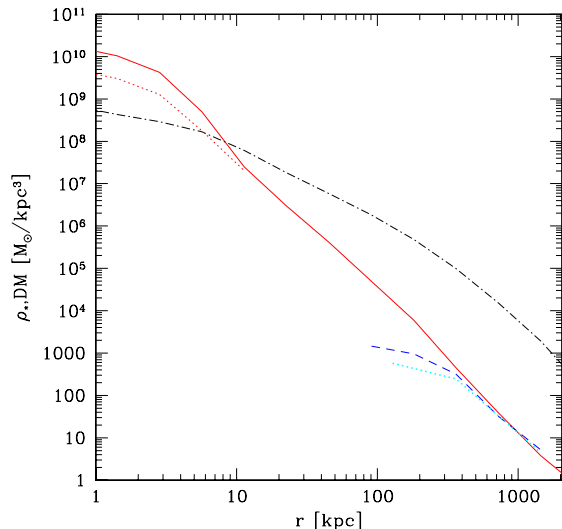


**Figure 11.** Spherically averaged density profiles for cluster C1 of cD+IC stars (solid line), dark matter (dot-dashed line), stars in cluster galaxies (dashed line) and, with arbitrary normalization, number density of cluster galaxies (dotted line). The result of applying the correction for the excess, young central stars is shown by the thin, dotted line.

The projected stellar velocity dispersion is 350-400 km/s at the center of the cD, increases to  $\sim 500$  km/s at  $R \sim 10$ -30 kpc and then decreases gradually with increasing  $R$  to about 300 km/s at  $R_{\text{vir}}$ . An increase of the stellar velocity dispersion with  $R$  has been observed in some cDs, such as A2029 (Dressler 1979), and has been interpreted as marking the transition from galactic to intracluster stars. The effect is less pronounced after correction for the excess young central stars, but we note that these stars still contribute to the gravitational potential and therefore boost the central velocity dispersions. The projected velocity dispersion of the dark matter follows a similar trend with  $R$  as that of the stars, but is significantly larger. As the stars and dark matter are moving in the same gravitational potential this implies that the density distribution of dark matter is significantly flatter than that of the cD+IC stars — see below.

The projected velocity dispersions along the major axis of the cD are shown by solid lines. They have been calculated as the average of the projected velocity dispersions along the x-axis and y-axis. Along the x-axis the velocity dispersions are calculated for stars and dark matter particles projecting onto  $\pm 30$  deg. wedges along the positive and negative y directions, and vice versa for dispersions along the y-axis. The major axis velocity dispersions follow similar trends as the minor axis ones. However, for the cD+IC stars it is significantly larger and for the dark matter halo somewhat larger than along the minor axis. This shows that both systems are flattened by anisotropic velocity dispersions and, as stated above, oriented in similar ways. For cluster C2 the findings are similar (not shown) though the cD is not aligned with the cluster in this case and both systems are only mildly flattened.



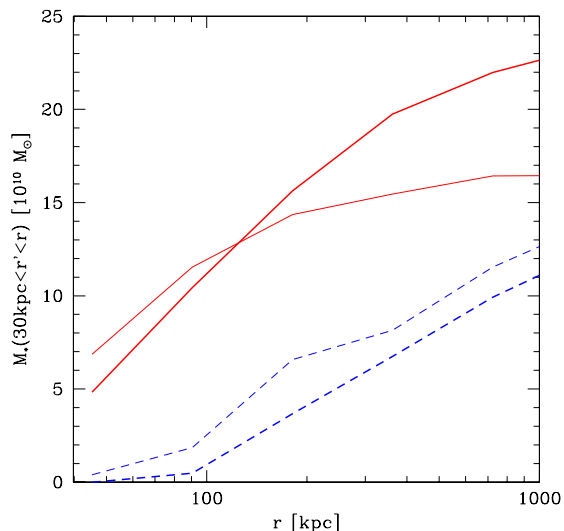


**Figure 12.** For a  $M_{\text{vir}}=3.4 \times 10^{13} h^{-1} M_{\odot}$  ( $T=1.1$  keV) group is shown at  $z=0.1$  the cumulative mass in cD+IC stars (solid lines) and in stars in cluster galaxies (dashed lines) outside of  $r=30$  kpc for the normal resolution (thin lines) and high resolution (thick lines) simulations, respectively.

Summarizing our findings for the Virgo-like cluster, the typical projected velocity dispersion for the cD+IC stars at  $R \gtrsim 50$  kpc is 300-600 km/s depending on orientation and projected distance from the cluster center. Freeman et al. (2000) find a (projected) velocity dispersion of  $752 \pm 110$  km/s for 23 IC planetary nebulae in the Virgo-cluster at a projected distance of about 150 kpc from M87. This value is somewhat larger than our prediction, but it may be due to the “real” Virgo-cluster being kinematically unrelaxed (see also section 3.3); the observational sample is too small to test for velocity substructure (Freeman 2004, private communication).

Since clusters are dynamically fairly young it is important to establish that the results on kinematics etc. are robust, i.e. they do not depend on the particular frame chosen for the analysis. To this end we analyzed for each cluster two frames 1.5 and 3 Gyr before the present time, corresponding to redshifts 0.12 and 0.26, respectively. We find that none of the results presented in this paper change in any significant way when going to these earlier frames.

### 3.6 Density Distributions of the Intracluster Stars, Cluster Galaxies and the Dark Matter

In Figure 11 we show for cluster C1 the spherically averaged density distributions of the cD+IC stars (with and without the correction for the excess, young central stars), the stars in cluster galaxies, the dark matter and, with an arbitrary normalization, the *number* density of cluster galaxies. As suggested previously, the number density profile of cluster galaxies in the inner parts of the cluster as well as the dark matter density profile in general are significantly flatter than the density profile of cD+IC stars. For the cluster galaxies

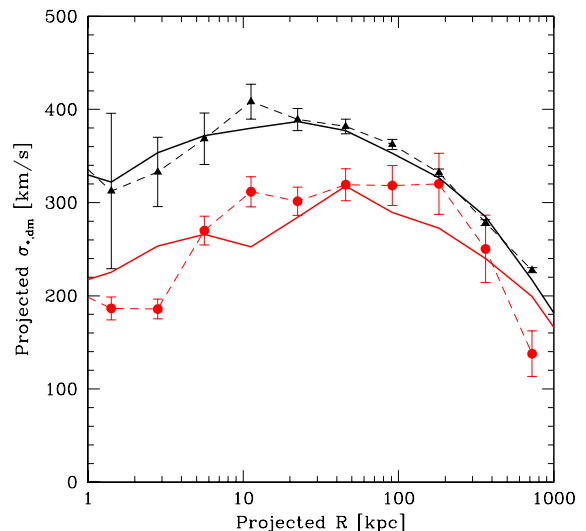


**Figure 13.** Velocity dispersions projected along the minor axis of the “cD” for the cD+IC stars (lower curves and symbols) and dark matter (upper curves and symbols) in the group. Results for the normal resolution simulation are connected by dashed lines and are shown as solid circles with errorbars (stars) and solid triangles with errorbars (dark matter). Results for the high resolution simulation are shown by solid lines.

this is a manifestation of the transformation of galaxies to cD+IC stars by tidal disruption in the inner parts of the cluster.

Moreover, it follows from Fig.11 that the average (mass) density of stars in cluster galaxies only exceeds that of the IC stars beyond about half the virial radius - this is in good agreement with the findings of Murante et al. (2004).

### 3.7 A Numerical Resolution Test

It is important to test whether the results presented in this paper depend on the numerical resolution of the simulations. To this end we carried out one simulation with eight times higher mass and two times higher force resolution. This results in particle masses of  $m_{\text{gas}}=m_{*}=3.1 \times 10^7$  and  $m_{\text{DM}}=2.3 \times 10^8 h^{-1} M_{\odot}$  and gravity softening lengths of 1.4, 1.4 and  $2.7 h^{-1}$  kpc, respectively. Due to computational limitations we ran the high resolution simulation for a group of virial mass  $3.4 \times 10^{13} h^{-1} M_{\odot}$  and emission weighted temperature 1.1 keV, rather than for clusters C1 and C2. In order to enable an optimal comparison between the normal and high resolution runs only Fourier modes up to the Nyquist wavenumber of the normal resolution simulation were used to prepare the initial conditions for the high resolution run (i.e., additional high-wavenumber modes up to the Nyquist wavenumber of the high resolution simulation were *not* added to the Fourier modes). We shall denote in the following the central galaxy in the group the “cD”. In Figure 12 we show the cumulative mass of cD+IC stars and stars in galaxies outside of  $r=30$  kpc for the normal and high resolution runs at  $z=0.1$  (at  $z=0$  one large group galaxy is

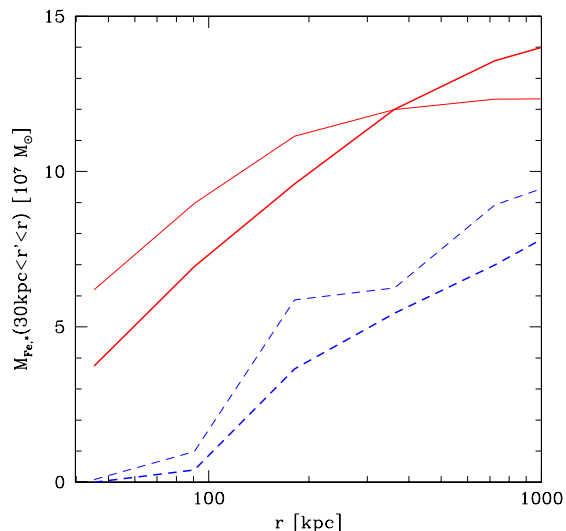


**Figure 14.** Same as Figure 12, except that cumulative masses of Iron are shown.

merging with the cD). There is reasonable agreement between the runs — the somewhat larger mass in IC stars in the high resolution simulation at  $r \gtrsim 200\text{--}300$  kpc is likely due to the better resolution of star-forming gas in the lower over-density regions which come to populate the outer parts of the group.

As one goes to higher resolution one might naively expect that the fraction of IC stars in the simulations decreases as the cluster galaxies are increasingly well resolved. The interesting indication from Figure 12 is, however, that if anything the fraction of IC stars slightly *increases* with increasing numerical resolution.

Shown in Figure 13 at  $z=0.1$  are the azimuthally averaged velocity dispersions of cD+IC stars and dark matter projected along the minor axis of the cD for the normal and high resolution simulations, and with the correction for excess young central stars discussed previously applied. The agreement is overall reasonable, especially when it is taken into account that there are at  $z=0.1$  just 1235 cD+IC stars inside of the virial radius in the normal resolution simulation of this group. This is a factor 10-20 less than the corresponding numbers for clusters C1 and C2. The increase in central velocity dispersion ( $R \lesssim 10$  kpc) for the high resolution simulation, in particular for the stars, is likely an effect of the increased force resolution.

Finally, as a test of resolution dependence of chemical evolution and abundances we show in Figure 14 the cumulative mass of Iron in cD+IC stars and stars in galaxies outside of  $r=30$  kpc for the normal and high resolution runs at  $z=0.1$ . There is reasonable agreement between the runs and we note that in relation to Figure 12 this is a nontrivial result, since a significant fraction of the iron produced by the stars ends up in the hot ICM (Romeo et al. 2004).

In general, as mentioned at the beginning of section 3, we carry out all the analysis of the (normal resolution) cluster simulations C1 and C2 presented in this paper for

the normal and high resolution group simulations also. On this basis we find that all results given in this paper appear largely robust to resolution changes. Ultimately, however, this can only be properly checked by running the “production” simulations C1 and C2 at higher numerical resolution — see below.

## 4 CONCLUSIONS

In this paper we have discussed the properties of the intracluster (IC) stellar populations. Our results are based on cosmological simulations of galaxy clusters including self-consistently metal-dependent atomic radiative cooling, star-formation, supernova driven galactic super-winds, non-instantaneous chemical evolution and the effects of a meta-galactic, redshift dependent UV field. In relation to modelling the properties of the IC stars this is an important step forward with respect to previous theoretical works on the subject which were based on purely N-body (collisionless) simulations, apart from the recent, interesting work by Murante et al. (2004).

The main results from our simulations of a Virgo-like (C1) and a (sub) Coma-like (C2) galaxy cluster regarding the IC stellar populations are as follows:

The intracluster (IC) stars are found to contribute 20-40% of the total cluster B-band luminosity at  $z=0$  and to form at a mean redshift  $\bar{z}_f \sim 3$  somewhat larger than the mean formation redshift of the stars in cluster galaxies of about 2.5. This difference corresponds to a time span of about 0.5 Gyr. Murante et al. (2004) find mean formation redshifts of 1.5 and 1.2, respectively — the reason for this discrepancy between the two works remains to be identified.

We calculate UBVRIJHK surface brightness profiles of the IC star populations and find that the profile of the larger cluster matches the observed V-band profile of Abell 1413 ( $T \simeq 8$  keV) quite well. For the Virgo-like cluster we fail, however, to match the flat profile between 200 and 400 kpc projected cluster-centric distance observationally (but indirectly) inferred for the Virgo cluster by Arnaboldi et al. (2002) using planetary nebulae. We note though that the galaxy distribution in Virgo is also unusually flat (Binggeli et al. 1987). The V-band surface brightness is found to reach  $V_{lim} \simeq 28.3$  mag/arcsec<sup>2</sup> (Feldmeier et al. 2002) in cluster C2 at  $r \sim 350$  kpc and in cluster C1 at  $r \sim 250$  kpc. The typical colour of the IC stars is B-R=1.4-1.5, comparable to the colour of larger elliptical galaxies and in qualitative agreement with the observational findings of Gonzalez et al. (2000) for the rich cluster Abell 1651.. The mean Iron abundance of the IC stars is about solar in the central part of the cluster ( $r \sim 100$  kpc) gently decreasing to about half solar at the virial radius. The IC stars are  $\alpha$ -element enhanced with, e.g. [O/Fe] increasing slightly with  $r$  and characterized by a typical [O/Fe] $\sim 0.4$  dex.

The IC stars are kinematically significantly colder than the cluster galaxies: The velocity dispersions of the IC stars are in the inner parts of the cluster ( $r \sim 100\text{--}500$  kpc) only about half of those of the cluster galaxies increasing slightly to about 70% at  $r=1\text{--}2$  Mpc. The typical projected velocity dispersion in the Virgo-like cluster at  $R \gtrsim 50$  kpc is 300-600 km/s depending on orientation and projected distance from the cluster center. Rotation is found to be dynamically

insignificant for the IC stars. The velocity distributions of IC stars *and* clusters galaxies are in one cluster highly radially anisotropic, in the other close to isotropic.

A test simulation of a  $T \simeq 1.1$  keV group at higher numerical resolution indicates that the results presented are largely robust to resolution changes. Work is in progress to simulate also at higher resolution the two clusters discussed in this paper. Moreover, we are in the process of enlarging significantly our sample of galaxy clusters.

## ACKNOWLEDGEMENTS

We have benefited considerably from discussions with Magda Arnaboldi, Giuseppe Murante and Ken Freeman. All computations reported in this paper were performed on the IBM SP4 facility provided by Danish Center for Super Computing (DCSC). We gratefully acknowledge the abundant access to computing time on this system. This work was supported by Danmarks Grundforskningsfond through its support for the establishment of the Theoretical Astrophysics Center (TAC).

## REFERENCES

Arnaboldi, M., 2004, IAU Symp., **217**, Recycling intergalactic and interstellar matter, in press (astro-ph/0310143)  
 Arnaboldi, M. et al., 2002, AJ, 123, 760  
 Arnaboldi, M. et al., 2003, AJ, 125, 514  
 Binggeli, B., Tammann, G.A., & Sandage, A., 1987, AJ, 94, 251  
 Binney, J., & Tremaine, S. 1987, Galactic Dynamics. Princeton Univ. Press, Princeton  
 Borgani, S., 2004, MNRAS, in press (astro-ph/0310794)  
 Cleary, P. W., & Monaghan, J. J., 1999, Journal of Computational Physics, 148, 227  
 Dressler, A., 1979, ApJ, 231, 659  
 Dubinski, J., 1998, ApJ, 502, 141  
 Durrell, P.R., Ciardullo, R., Feldmeier, J.J., Jacoby, G.H., & Sigurdsson, S., 2002, ApJ, 570, 119  
 Ettori, S., & Fabian, A.C., 2000, MNRAS, 317, 57  
 Feldmeier, J.J., et al., 2002, ApJ, 575, 779  
 Ferguson, A.M.N., Irwin, M.J., Ibata, R.A., Lewis, G.F., & Tanvir, N.R., 2002, AJ, 124, 1452  
 Freeman, K.C., et al., 2000, ASP Conf. Series, 197, 389  
 Gal-Yam, A., et al., 2003, AJ, 125, 1087  
 Girardi, L., et al., 2002, A&A, 391, 191  
 Gladders, M.D., et al., 1998, ApJ, 501, 571  
 Gonzalez, A.H, et al., 2002, ApJ, 536, 561  
 Helmi, A., White, S.D.M., de Zeeuw, P.T., & Zhao, H., 1999, Nature, 402, 53  
 Helmi, A., White, S.D.M., & Springel, V., 2003, MNRAS, 339, 834  
 Lia, C., Portinari, L., & Carraro, G. 2002, MNRAS, 330, 821  
 McNamara, B. R., 2004, in “The Riddle of Cooling Flows in Galaxies and Clusters of Galaxies”, Charlottesville, Virginia, USA, Eds. T.H.Ruprecht, J.C.Kempner & N.Soker  
 Mori, M., Yoshii, Y., Tsujimoto, T., & Nomoto, K. 1997, ApJ, 478, L21

Murante, G., et al., 2004, ApJL, submitted  
 Napolitano, N.R., et al., 2003, ApJ, 594, 172  
 Oemler, A. Jr., 1976, ApJ, 209, 693  
 Romeo, A.D., Sommer-Larsen, J., Portinari, L., & Antonuccio, V., 2004, MNRAS, in preparation  
 Sommer-Larsen J., Götz M., Portinari L., 2003, ApJ, 596, 46  
 Springel, V., & Hernquist, L., 2003, MNRAS, 339, 312  
 Tornatore, L., Borgani, S., Matteucci, F., Recchi, S., & Tozzi, P., 2004, MNRAS, in press (astro-ph/0401576)  
 Valdarnini, R., 2003, MNRAS, 339, 1117